Enhanced Carrier Confinement and Mode Discrimination for Laterally-Coupled DFB Lasers

Kun Tian, Yonggang Zou, Mingyue Guan, Linlin Shi, He Zhang, Yingtian Xu, Jie Fan, Hui Tang, and Xiaohui Ma

***Abstract*—Reducing carrier leakage is the key to obtain laterally coupled distributed feedback (DFB) lasers with high injection efficiency. We proposed a device structure with slots fabricated between the ridge and gratings to form a good confinement on carriers. The incorporation of slots also makes the grating morphology easier to fabricate. To evaluate the dependence of coupling efficient on main structural parameters, four grating samples with different sizes are studied with FDTD Solutions. Calculation results indicate that slots with a width of $0.1-0.3\ \mu m$ is suitable for the device. And, changing the lateral width of the grating can be used as a direct method to adjust the coupling strength. In addition, the carrier distribution and optical field distribution of the device were simulated with Crosslight PICS3D, and the results show that compared with the traditional laterally-coupled gratings, this structure can strengthen the competitive advantage of fundamental mode and enhance the mode discrimination of the device. This structural design provides ideas and references for improving the injection efficiency and mode stability of laterally-coupled DFB lasers.**

***Index Terms*—DFB lasers, gratings, narrow slots, coupling coefficient.**

I. Introduction

DISTRIBUTED feedback lasers [1] play an important role in many fields, such as optical fiber communication, tunable diode laser absorption spectroscopy, chip scale atomic clock, ellipsometry and 3D vision due to their good monochromaticity (spectral purity), narrow linewidth (within 1 MHz) and high side mode suppression ratio (SMSR $>$ 45 dB). Buried gratings are the key element to realize wavelength selection and good mode characteristics of the device [2], but their fabrication process generally involves growth interruption and re-growth. The process of regrowth introduces extra problems, such as surface damage induced by etching as well as the introduction of impurities and defects. Thus, the regrowth-free device can greatly simplify the process and reduce the manufacturing cost. The raised problem is solved by the surface grating [3], [4]. For many devices, it can be easily etched into the surface of the completely epitaxial wafer, which avoids epitaxial overgrowth and facilitates the fabrication of the device. Surface gratings have two particularities. Firstly, in contrast to the buried grating, the surface grating usually requires a large etching depth to increase the overlap between the grating region and the transverse optical field to gain sufficient coupling. Secondly, after fabrication, it is necessary to fill the grating groove with dielectric materials, such as SiO_2, Si_3N_4 or benzocyclobutene (BCB), and then open an electrode window on the grating ridge to inject carriers, which is the normal fabrication process of such devices.

There exists a pair of contradictions in the structural design of surface gratings. Usually, electrodes are fabricated in the unetched areas of the grating. In order to achieve cost-effective mass production, surface gratings with too small order or period should be avoided, because they increase the difficulty of processing the electrode window. And, electrodes with too narrow width can also lead to increased electrical resistance. In addition, for large period gratings, the radiation loss increases with the growth of the order, which degrades the performance of DFB lasers. The proposal of the laterally-coupled ridge-waveguide (LC-RWG) surface gratings [5] deal with it. LC gratings are defined in the ridge sidewalls to interact with the lateral evanescent field, and there is a clear boundary between the current injection region and the grating region. This design not only eliminates the requirement for the grating order, but also reduces the influence of the current carrier on the grating. However, during the etching process, aspect-ratio-dependent-etching (ARDE) effect gives rise to the imperfect profile of the grating. The portion of the grating groove bottom near the center of the waveguide mode field is not fully etched to the desired shape. This is where the interaction between the optical field and the grating is strongest. The structural deviation leads to an uncontrollable decrease in the coupling coefficient κ and affects the effective refractive index of the waveguide. Although enlarging the lateral size of LC grating can compensate for the decrease of κ, it reduces the injection efficiency and increases the threshold current, due to the increased lateral leakage of the pump current. In recent years, the structural innovation and performance optimization of this laser have been carried out. Most research focused on expansion of working wavelengths [6], [7], [8], grating material [9], grating structure [10], device function [11] and others [12],

Manuscript received March 11, 2022; revised May 20, 2022; accepted June 2, 2022. Date of publication June 8, 2022; date of current version June 21, 2022. This work was supported in part by the National Natural Science Foundation of China under Grants 61804013, 61804014, 61805023, and in part by the Department of Science and Technology, Jilin Province, under Grants 20190302052GX and 20210201030GX. *(Corresponding author: Yonggang Zou.)*

Kun Tian, Yonggang Zou, Linlin Shi, He Zhang, Yingtian Xu, Jie Fan, Hui Tang, and Xiaohui Ma are with the Changchun University of Science and Technology, Changchun, Jilin 130000, China (e-mail: 276322455@qq.com; zouyg@cust.edu.cn; shilinlin@cust.edu.cn; zhanghe@cust.edu.cn; xyt@cust.edu.cn; fanjie@cust.edu.cn; 2435763337@qq.com; mxh@cust.edu.cn).

Mingyue Guan is with the Tsinghua–UC Berkeley Shenzhen Institute, Shenzhen 518055, China (e-mail: guanmy17@mails.tsinghua.edu.cn).

Digital Object Identifier 10.1109/JPHOT.2022.3180756

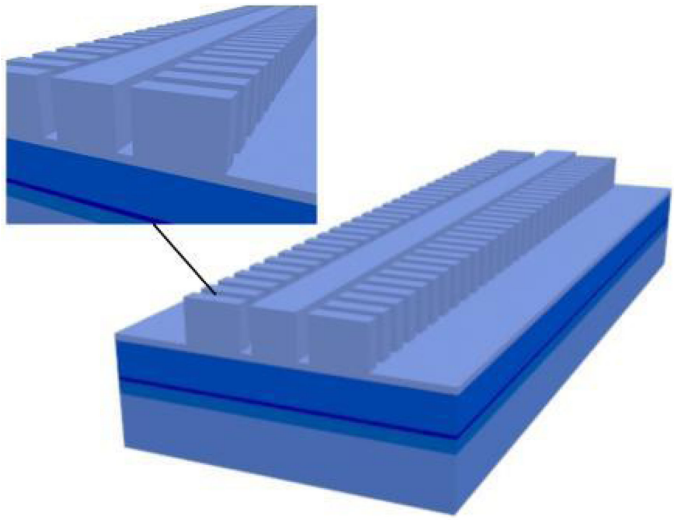

Fig. 1. Schematic diagram of a LC-RWG DFB structure with slots fabricated between the ridge and gratings.

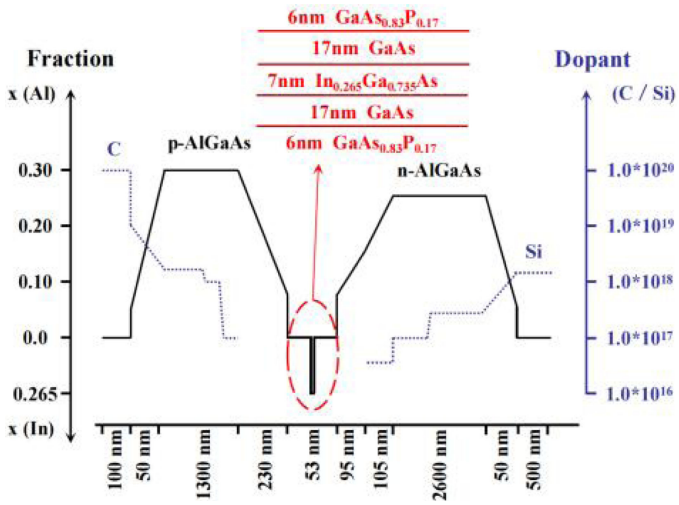

Fig. 2. The epitaxial structure for LC-RWG DFB lasers.

[13]. However, in view of the above problems, there are still no efficient solutions.

The structure proposed in this paper circumvents these problems by introducing a slot between the unetched ridge and LC gratings, which strengthens the restriction of the carriers flowing to the LC grating. The effects of structural parameters on the coupling coefficient and effective refractive index of the grating, as well as the coupling between carriers and optical field are studied by simulation.

II. Device Structure

The DFB structure has a deep narrow slot between the ridge and gratings, as shown in Fig. 1. Grating etching can be carried out after the fabrication of ridge and slot, which helps to avoid the non-ideal structure profile caused by ARDE effect in the process of etching grooves. Furthermore, another benefit of this structure is that the slot etching and the filling of dielectric material can reduce the lateral leakage of carriers.

The full vertical structure of epitaxial wafer is shown schematically in Fig. 2. An aluminum-free separate confinement heterostructure (SCH) consists of a single 7 nm thick undoped $In_{0.265}Ga_{0.735}As$ quantum well (QW) and two 17 nm thick undoped GaAs quantum barrier layers. By placing a 6nm GaAsP material layer between the quantum barrier and waveguide layer, the lattice stress is relieved. The QW layers are embeded between asymmetric undoped waveguides, and the Al composition of the waveguides is gradually changed. In addition, asymmetric cladding layers are adopted to reduce the absorption loss of device and to increase the confinement factor difference between the fundamental mode and higher-order modes, so as to realize a stable operation of device. The implemented LC grating is 1st order, leading to a period of about 0.16 μm according to the Bragg condition ($\lambda_{Bragg} = 1.064\,\mu$m).

III. Result and Analysis

A. Simulation Model

Fig. 3 shows a cross-sectional view (a) and a top view (b) of device structure. In the fabrication process, preference can be given to the fabrication of ridge and slots, and then etching the grating separately, which is beneficial to reducing the influence of etching process on other structures. After that, the space around the grating is filled with silicon oxide. The changes of the structural parameters of the grating and ridge will have different effects on the optical mode distribution and carrier distribution of the device. Here, we mainly study five parameters: slot width W_s, residual layer thickness of the slot D_s (the distance from the slot bottom to the waveguide), grating width W_g, grating height H_g (the length from the top of grating to the bottom) and ridge width W_r.

The simulation model of LC-RWG grating with slots is established by using MODE Solutions [14]. In the calculation, the structure is simplified and the electrode contacts and cap layers are removed because their influence on the grating coupling coefficient is small. The fundamental mode is employed in the simulation and the grid sizes of longitudinal, lateral and transverse direction are 0.02 μm, 0.025 μm and 0.025 μm. The initial settings of parameters are: $W_r = 2\,\mu$m, $W_g = 2.5\,\mu$m and $W_t = 15\,\mu$m.

Many evidence [15], [16], [17] point out that the precise control and calibration of κ is crucial to the design and fabrication of DFB lasers. Under the condition of keeping the cavity length constant, the grating with low κ can not provide enough feedback and mode selectivity, while the grating with high κ always leads to spatial hole burning and the decrease of SMSR. The κ L studied in this paper is designed to be 1.25. For a typical 500 μm cavity length and the coupling coefficient of the LC grating is 25cm^{-1}, the reflectivity of the corresponding passive grating is 0.71858, as shown in Fig. 3(c). In addition, another research object in this paper is the effective refractive index of the device, which determines the Bragg wavelength. Therefore,

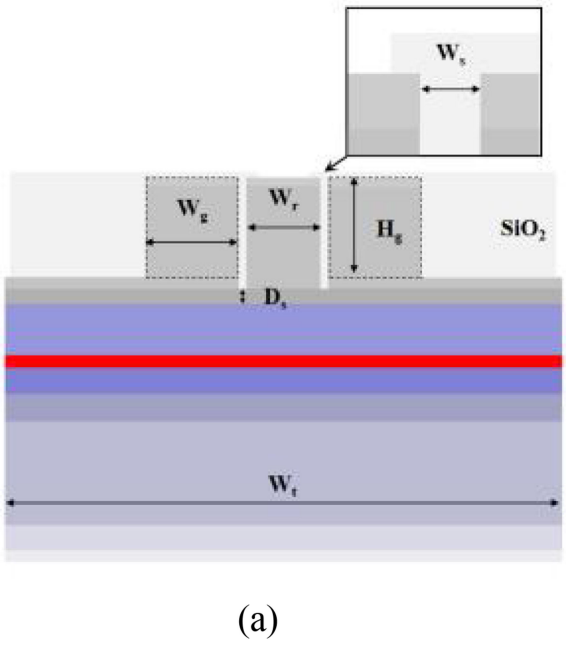

(a)

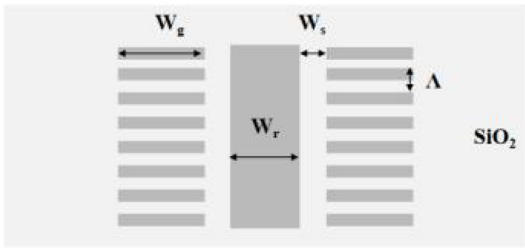

(b)

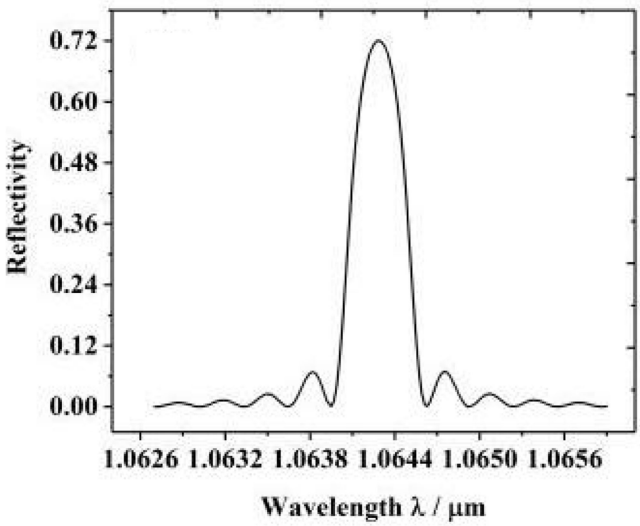

(c)

Fig. 3. (a) Schematic cross-seciton of LC-RWG grating with slots set in both sides of ridge; (b) Top view of the LC-RWG grating and ridge; (c) The reflection spectrum of DFB grating with $L_{cavity} = 500\ \mu$m and $\kappa = 25\ cm^{-1}$.

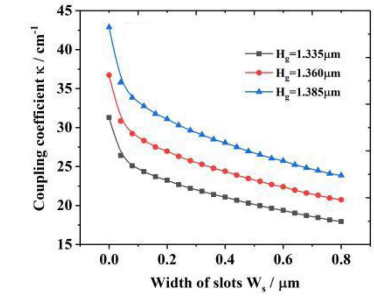

(a)

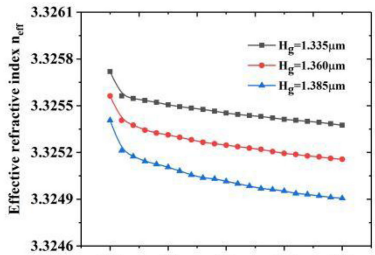

(b)

Fig. 4. The dependence of κ (a) and n_{eff} (b) on slots width.

it is of great significance to study the influence of the change of device structure on them, which is helpful to realize the accurate adjustment of λ_{Bragg}.

B. Dependence of κ and N_{eff} on Slots Structure

The width of slots between the unetched ridge and LC grating is gradually increased from 0 μm to 0.8 μm, that is, the grating gradually moves to the outside of the ridge, to investigate the influence of slot width on the κ of the grating and the n_{eff} of the waveguide. Three kinds of gratings with different heights H_g (1.380 μm, 1.355 μm and 1.330 μm) were selected for comparative study.

Fig. 4 shows that κ and n_{eff} decrease with the increase of slot width W_s. This is because the enlarged slot width reduces the overlap between the grating and the optical field. And, the widening of slots filled with SiO_2 increases its overlap with the optical field, lowering the n_{eff} of waveguide. Apparently, a narrower slots leads to the higher sensitivity of κ and n_{eff} to W_s variation. When W_s increases more than 100 nm, the reduction of κ and n_{eff} slows down. In addition, the higher the LC grating, the stronger the grating optical confinement. In other words, the smaller the grating residual layer thickness, the more light field leaks into the grating area, which promotes the increase of κ. It also can be seen that with the increase of W_s, the decrement of κ and n_{eff} is smaller for the grating with higher H_g. The data in the figure also means that the slot with a very narrow width ($<$ 80 nm $=$ width of grating grooves) helps to achieve high κ, However, the fabrication error can easily lead to obvious changes in κ and n_{eff}, which brings instability to the threshold gain and emission wavelength of the device, so it is not ideal for the device. To obtain the κ of the target, larger W_s corresponds to higher H_g. However, for the deeper grating, it is necessary

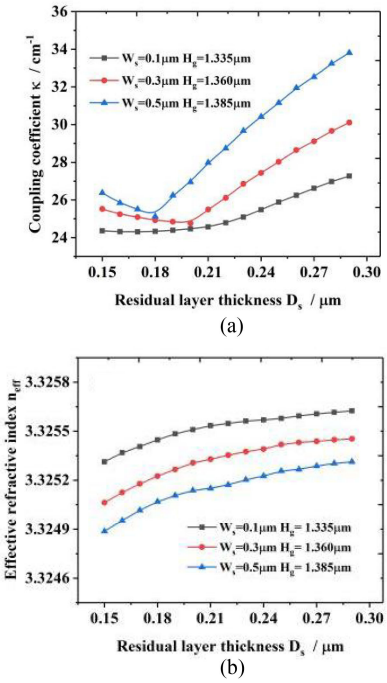

Fig. 5. The dependece of κ (a) and n_{eff} (b) on the residual layer thickness of slots D_s.

to readjust the waveguide structure to obtain the target value of wavelength which is determined by the n_{eff}. So, setting W_s in a reasonable range (0.1∼0.5 μm) is of great significance to the design and fabrication of the device.

The calculation results in Fig. 4. are based on the setting $D_s = D_g$ (the distance from grating groove bottom to waveguide layer). In fact, the value of D_s also affect the function of grating. So, three gratings with different structural parameters ($W_s = 0.1\ \mu$m and $H_g = 1.335\ \mu$m, $W_s = 0.3\ \mu$m and $H_g = 1.360\ \mu$m, $W_s = 0.5\mu$m and $H_g = 1.385\ \mu$m) are designed to investigate the dependence of κ and n_{eff} on D_s. It should be mentioned in advance that the coupling coefficients of these three gratings are about 25 cm^{-1}.

The κ and n_{eff} as a function of the residual layer thickness of slots D_s are illustrated in Fig. 5. The increase of D_s, relative to the reference value, leads to a larger κ since the rise of slots bottom lowers the optical confinement of ridge and increases the overlap of optical field with gratings. Conversely, deepening the slots can weaken the coupling between the grating with the optical mode, but the optical field deformation caused by it may expands κ for some structures with $W_s = 0.3\ \mu$m and 0.5 μm. In addition. For n_{eff}, the decrease of slots D_s gives a larger overlap between the slot region with the optical field, resulting into a reduced n_{eff}.

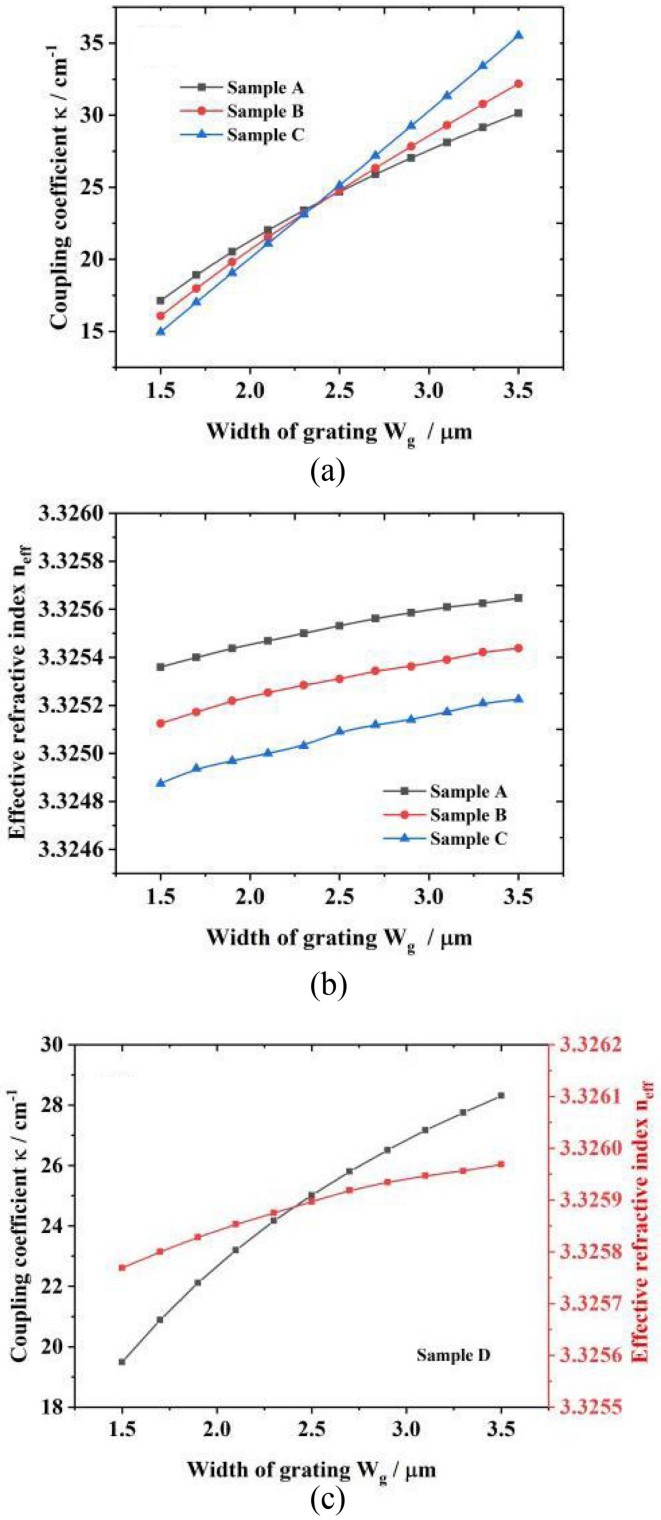

Fig. 6. κ (a) and n_{eff} (b) dependence on grating width W_g and these dependence for sample D (c).

C. Dependence of κ on Grating and Ridge Structures

On the ground of above law, in order to reduce the process complexity of the device, we set the grating grooves bottom at the same height with slot bottom and take this relationship as the basic setup of the following simulation. To evaluate the influence of geometry variations on the coupling characteristics, four grating samples are selected and optimized, as is shown in Table I.

Fig. 6(a) and (b) show the dependence of κ and n_{eff} on grating width W_g (from 1.5 μm to 3.5 μm), respectively. These dependence of sample D in Fig. 6(c) are for comparisons.

TABLE I
FOUR SAMPLES OF LC-RWG GRATINGS WITH DIFFERENT PARAMETERS

Samples	A	B	C	D
W_s	0.1μm	0.3μm	0.5μm	0μm (without slots)
D_s	0.220μm	0.200μm	0.180μm	0.253μm
n_{eff}	3.3254	3.3252	3.325	3.3259
κ	≈24.79cm^{-1}	≈24.77cm^{-1}	≈25.13cm^{-1}	≈25.03cm^{-1}

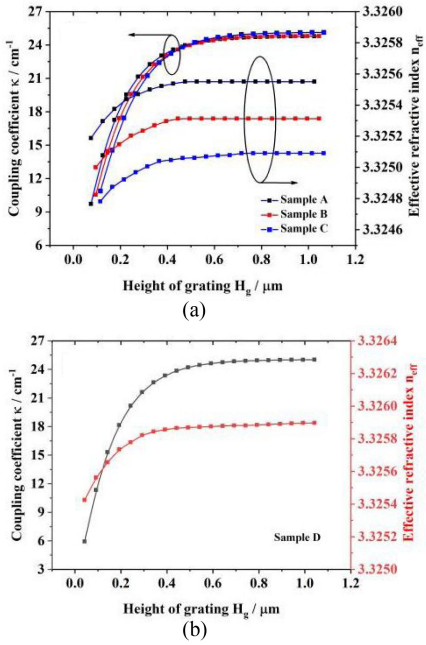

Fig. 7. κ and n_{eff} dependence on grating width H_g (a) and these dependence for sample D (b).

It is clear that in Fig. 6(a), κ increases significantly with the increase of the lateral width of LC grating W_g and the same trend also occurs in Fig. 6(b) and (c). This is because the extension of W_g brings about an improved optical confinement factor of the grating and the enlargement of waveguide in the lateral direction, thus increasing κ and n_{eff} respectively. Moreover, it is apparent that larger W_s gives rise to higher growth rate. The growth rates of κ for four samples are $6.51*10^{-4}$ cm^{-2} (A), $8.06*10^{-4}$ cm^{-2} (B), $10.29*10^{-4}$ cm^{-2} (C) and $4.41*10^{-4}$ cm^{-2} (D) respectively. The reason may be that increasing W_s and adding the depth of slots as well as gratings will weaken the lateral confinement of waveguide ridge on the optical mode and hence, as W_g increase, more optical field is attracted into grating area. However, The small growth rates of n_{eff} for the 4 samples are $1.44*10^{-4}$ cm^{-1} (A), $1.56*10^{-4}$ cm^{-1} (B), $1.75*10^{-4}$ cm^{-1} (C) and $1*10^{-4}$ cm^{-1} (D) respectively. These results illustrate that broadening W_g can serve as a feasible way to improve κ , and a narrow slot may be a good choice if the precise tailoring of κ is desired.

Fig. 7 presents the effect of grating height H_g on κ and n_{eff}. In investigation, the position of grating grooves bottom is kept and the position of the top is variable.

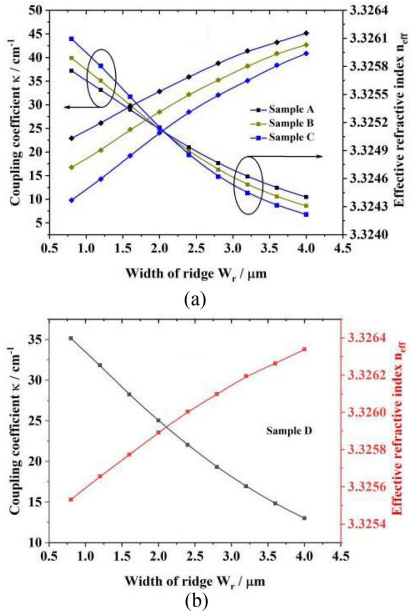

Fig. 8. The dependence of κ and n_{eff} on W_r. (a) LC gratings with slots; (b) Conventional LC gratings.

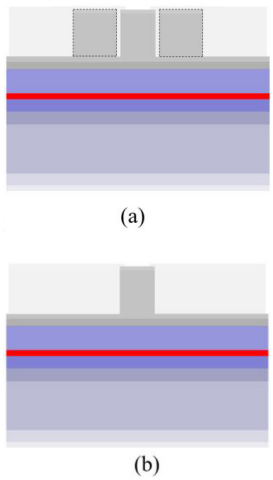

Fig. 9. Wide section (a) and narrow section (b) of LC gratings. (Dotted lines delimit the grating areas).

With the drop of grating top, κ and n_{eff} decline, and their variation values are very close. In the process of H_g decreasing to about 0.6 μm, the diminution of κ and n_{eff} is very small, while in the range from 0.6 μm to 0.1 μm, both of them decrease at an ever-growingly fast speed. This is because the optical field in the grating region quickly decays from the bottom up and the field intensity near the top of cladding is very weak, so that a small scale drop of H_g has little effect on the overall optical field distribution and κ. It can also be seen in Fig. 7 that the variation amplitude of κ and n_{eff} of conventional LC DFB close to that of LC DFB with slots which means that in transverse direction, the optical field distribution in grating regions of four samples is very similar.

Based on the distribution characteristics of optical field in grating region, a new type of device structure can be developed.

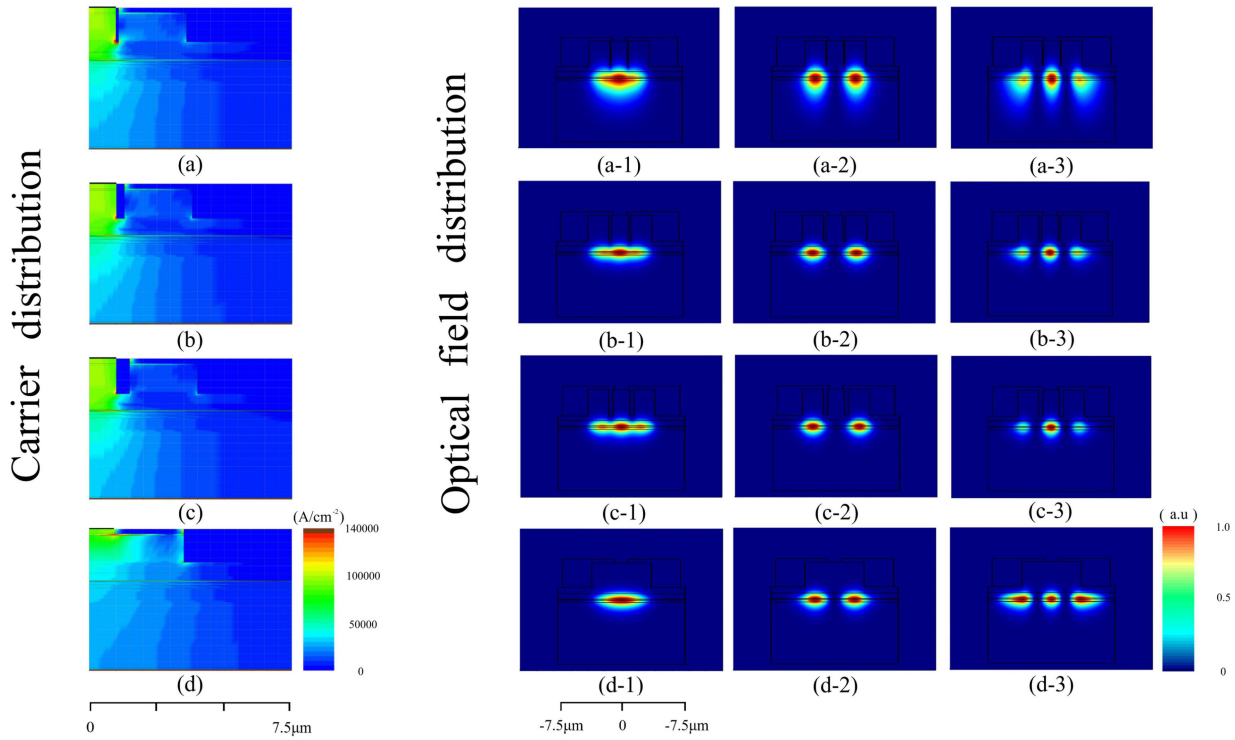

Fig. 10. Carrier distribution in four sample lasers (left panel). (a) Semi structure of A, (b) Semi structure of B, (c) Semi structure of C, (d) Semi structure of D; Optical field distribution of fundamental mode, first-order mode and second-order mode (right panel). The first column on the left panel shows the fundamental mode in four sample lasers, the second shows first-order mode and the third shows second-order mode. (The carrier distribution and three field distributions in a row belong to the same device).

In the structure, the grating has a smaller height than the ridge, which helps to decrease grating aspect ratio and the difficulty of etching process. It should be noted that compared with the traditional LC-RWG gratings, this design is more suitable for the structure with slots because of the easy fabrication of grating morphology.

Fig. 8 illustrates κ and n_{eff} as functions of W_r ranging from 0.8 to 4 μm. As can be seen, κ decreases and n_{eff} increases as W_r adds up. It implies that the width increase of ridge will strengthen its ability to confine the optical mode, reducing the overlap between the optical field and grating region, and hence, depressing κ and rising n_{eff}. It is significantly enlightening for us to realize that a narrower W_r speeds up the growth of κ, but raises the technical difficulty of obtaining an accurate κ value. Under the same process conditions, small W_r is not preferred for actual devices due to the high sensitivity of κ to W_r variation and low fabrication tolerance. And, it should be noted that too narrow a ridge brings high electrical resistance of device. The average rates of κ variation for four gratings are $8.35*10^{-4}$ cm^{-2}, $9.78*10^{-4}$ cm^{-2}, $11.62*10^{-4}$ cm^{-2} and $6.92*10^{-4}$ cm^{-2} respectively. For n_{eff}, the average rates are $3.516*10^{-4}$ cm^{-1}, $4.10156*10^{-4}$ cm^{-1}, $4.90234*10^{-4}$ cm^{-1} and $2.52*10^{-4}$ cm^{-1}. It can be concluded that the larger the W_s, the higher the slope of κ and n_{eff}.

D. Carrier Distribution and Optical Field Distribution

In the longitudinal direction of the cavity, the grating with slots can be divided into wide section and narrow section, as illustrated in Fig. 9. In conventional LC-RWG DFB lasers, some carriers transmitted downward in the ridge will spread to the lateral grating region. The resulting lateral leakage of pump current affects the refractive index of the grating and the injection efficiency as well as the threshold gain of the device. Since the narrow region structure of the four samples is the same, we select the wide section of gratings for modeling and analyze the carrier distribution and optical field distribution to qualitatively explain the benefits of the introduction of narrow slot to the device.

The carrier distributions of four samples are obtained by using Crosslight PICS3D [18], and the optical field distributions of the fundamental, first order and second order mode of 1.064 μm working wavelength are calculated by Mode Solutions.

The left panel of Fig. 10. shows the carrier distribution of the semi-structure of LC-RWG DFB lasers with slots, as well as that of conventional LC-RWG DFB lasers. The carrier distribution of LC-RWG DFB lasers with slots is obviously different from that of conventional lasers. In Fig. 10(a), (b) and (c), the carrier transmitted in the ridge is strongly confined by slots, and only a small number spread to the grating through the area below the slot bottom. In sample D, however, the lateral spreading of carrier to grating region on the both sides of ridge is obvious. What is more, there appears the aggregation of carriers at the lateral edge of the grating region and near the bottom of the p-cladding, the optical field intensity of the fundamental mode is weak here, which is opposite to that of the first and second-order modes. The coupling between carriers with high order modes in this region decreases the modal gain discrimination and the mode stability of the device. In addition, the lateral flowing

of carriers causes current leakage and the decline of injection efficiency. So, the introduction of the slot efficiently suppresses the lateral spreading of carriers, reduces the carrier density in the grating area, and weakens the phenomenon of carrier aggregation. Moreover, the variation of injected current will not lead to the obvious fluctuation of grating refractive index, which is beneficial to wavelength stability.

For optical field distributions, the increase of slot width and depth of the improves the confinement of waveguide structure on the optical mode in the transverse vertical direction, bringing about such an effect that the change of slot structure has a marked influence on the field distribution of first- and second-order mode. To be more specific, the growth of slot size increases the distance between the two intensity centers of the first-order mode field, and the field intensity in the middle is very weak, which enlarges the threshold gain of the first-order mode. For the second-order mode, there is a considerable overlap between the optical field in the waveguide and the ridge, which is helpful to obtain sufficient gain. However, with the increase of the slot size, the intensity of the optical field in the side grating decreases, resulting in insufficient feedback. So, the introduction of slots has a substantial influence on the distribution of carriers and optical field, which affects not only κ and n_{eff} but also lateral mode discrimination. To sum up, the introduction of the slot can not only reduce the leakage loss of current carrier, but also increase the mode stability of the device.

V. Conclusion

In order to reduce the influence of carrier leakage on device injection efficiency, we put forward a laterally coupled grating with narrow slots. Such grating design allows strengthened confinement of carrier by adding a slot between the ridge and gratings. Four samples with different slot sizes but similar coupling coefficients are applied to investigate the influence of grating and ridge structure parameters on grating coupling strength and effective refractive index. Calculation results indicate that LC-RWG gratings with slot width of 0.1-0.3 μm has a controllable coupling coefficient as well as strong mode discrimination ability to support stable fundamental-mode operation of LC DFB lasers. Moreover, adjusting the lateral width of grating is proven as a convenient and robust method of tailoring the coupling coefficient. Compared with the traditional laterally-coupled grating structure, this structure enhances the competitive advantage of the fundamental mode and the mode stability of the device.

References

[1] K. Sakai, K. Utaka, S. Akiba, and Y. Matsushima, "1.5 μm range InGaAsP/InP distributed feedback lasers," *IEEE J. Quantum Electron.*, vol. QE-18, no. 8, pp. 1272–1278, Aug. 1982, doi: 10.1109/JQE.1982.1071682.

[2] H. Nagai, T. Matsuoka, Y. Noguchi, Y. Suzuki, and Y. Yoshikuni, "InGaAsP/InP distributed feedback buried heterostructure lasers with both facets cleaved structure," *IEEE J. Quantum Electron.*, vol. QE-22, no. 3, pp. 450–457, Mar. 1986, doi: 10.1109/JQE.1986.1072981.

[3] D. Hofstetter, H. P. Zappe, J. E. Epler, and J. Söchtig, "Single-growth-step GaAs/AlGaAs distributed Bragg reflector lasers with holographically-defined recessed gratings," *Electron. Lett.*, vol. 30, no. 22, pp. 1858–1859, Oct. 1994, doi: 10.1049/el:19941262.

[4] R. M. Lammert, J. S. Hughes, S. D. Roh, M. L. Osowski, A. M. Jones, and J. J. Coleman, "Low-threshold narrow-linewidth InGaAs–GaAs ridge-waveguide DBR lasers with first-order surface gratings," *IEEE Photon. Technol. Lett.*, vol. 9, no. 2, pp. 149–151, Feb. 1997, doi: 10.1109/68.553068.

[5] F Pozzi, R. M. De La Rue, and M Sorel, "Dual-wavelength InAlGaAs-InP laterally coupled distributed feedback laser," *IEEE Photon. Technol. Lett.*, vol. 18, no. 24, pp. 2563–2565, Dec. 2006, doi: 10.1109/LPT.2006.887205.

[6] T. Feng *et al.*, "Laterally coupled distributed feedback type-I quantum well cascade diode lasers emitting near 3.22 μm," *Electron. Lett.*, vol. 56, no. 31, pp. H74–H80, Nov. 2017, doi: 10.1364/AO.56.000H74.

[7] J. H. Kang *et al.*, "Optically pumped DFB lasers based on GaN using 10th-order laterally coupled surface gratings," *IEEE Photon. Technol. Lett.*, vol. 29, no. 1, pp. 138–141, Jan. 2017, doi: 10.1109/LPT.2016.2630078.

[8] J. H. Kang *et al.*, "DFB laser diodes based on GaN using 10th order laterally coupled surface gratings," *IEEE Photon. Technol. Lett.*, vol. 30, no. 3, pp. 231–234, Feb. 2018, doi: 10.1109/LPT.2017.2780446.

[9] Y. Z. Song *et al.*, "Single mode 2 μm GaSb based laterally coupled distributed feedback quantum-well laser diodes with metal grating," *Chin. Phys. Lett.*, vol. 32, no. 7, Jul. 2015, Art. no. 074206, doi: 10.1088/0256-307X/32/7/074206.

[10] T. Loh, V. Krishnamurthy, and Q. Wang, "Design of laterally index-coupled grating III-V on Thin-SOI distributed feedback lasers," *IEEE Photon. Technol. Lett.*, vol. 27, no. 15, pp. 1624–1627, Aug. 2015, doi: 10.1109/lpt.2015.2432805.

[11] L. P. Hou, M. Haji, I. Eddie, H. L. Zhu, and J. H. Marsh, "Laterally coupled dual-grating distributed feedback lasers for generating mode-beat terahertz signals," *Opt. Lett.*, vol. 40, no. 2, pp. 182–185, Jan. 2015, doi: 10.1364/OL.40.000182.

[12] H. Virtanen, T. Uusitalo, M. Karjalainen, S. Ranta, J. Viheriälä, and M. Dumitrescu, "Narrow-linewidth 780-nm DFB lasers fabricated using nanoimprint lithography," *IEEE Photon. Technol. Lett.*, vol. 30, no. 1, pp. 51–54, Jan. 2018, doi: 10.1109/LPT.2017.2772337.

[13] S. Forouhar, R. M. Briggs, C. Frez, K. J. Franz, and A. Ksendzov, "High-power laterally coupled distributed-feedback GaSb-based diode lasers at 2 μm wavelength," *Appl. Phys. Lett.*, vol. 100, no. 3, Jan. 2012, Art. no. 031107, doi: 10.1063/1.3678187.

[14] MODE Solutions, Aug. 15, 2018. [Online]. Available: https://www.lumerical.com/cn/

[15] H. Soda, Y. Kotaki, H. Sudo, H. Ishikawa, S. Yamakoshi, and H. Imai, "Stability in single longitudinal mode operation in GaInAsP/InP phase-adjusted DFB lasers," *IEEE J. Quantum Electron.*, vol. QE-23, no. 6, pp. 804–814, Jun. 1987, doi: 10.1109/JQE.1987.1073454.

[16] J. E. A. Whiteaway, G. H. B. Thompson, A. J. Collar, and C. J. Armistead, "The design and assessment of λ/4 phase shifted DFB laser structures," *IEEE J. Quantum Electron.*, vol. 25, no. 6, pp. 1261–1279, Jun. 1989, doi: 10.1109/3.29257.

[17] K. David, G. Morthier, P. Vankwikelberge, R. G. Bates, T. Wolf, and B. Borchert, "Gain-coupled DFB lasers versus index-coupled and phase-shifted DFB lasers: A comparison based on spatial hole burning corrected yield," *IEEE J. Quantum Electron.*, vol. 27, no. 6, pp. 1714–1723, Jun. 1991, doi: 10.1109/3.89938.

[18] Crosslight PICS3D, Sep. 17, 2021. [Online]. Available: https://crosslight.com/applications/laser-diodes/